Accepted Manuscript

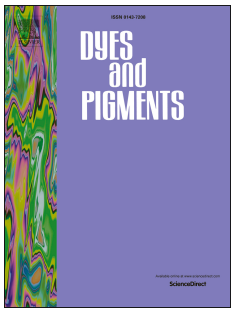

Direct connection of an amine to oligothiophene to generate push-pull chromophores for organic photovoltaic applications

Anubha Agarwal, Amanpreet Kaur Hundal, Jing-Yu Chen, Ante Bilic, Wanchun Xiang, Sheshanath V. Bhosale, Jing-Liang Li, Richard A. Evans, Akhil Gupta

PII: S0143-7208(18)31833-3

DOI: https://doi.org/10.1016/j.dyepig.2018.10.048

Reference: DYPI 7114

To appear in: *Dyes and Pigments*

Received Date: 18 August 2018

Revised Date: 22 October 2018

Accepted Date: 23 October 2018

Please cite this article as: Agarwal A, Hundal AK, Chen J-Y, Bilic A, Xiang W, Bhosale SV, Li J-L, Evans RA, Gupta A, Direct connection of an amine to oligothiophene to generate push-pull chromophores for organic photovoltaic applications, *Dyes and Pigments* (2018), doi: https://doi.org/10.1016/j.dyepig.2018.10.048.

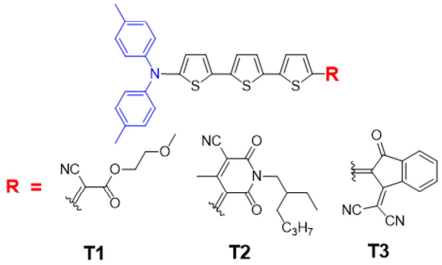

Push-pull donor chromophores for OPV applications
T3: $PC_{61}BM$ (1:1) = 6.12%

Direct connection of an amine to oligothiophene to generate push-pull chromophores for organic photovoltaic applications

Anubha Agarwal,[a] Amanpreet Kaur Hundal,[b] Jing-Yu Chen,[a] Ante Bilic,[c] Wanchun Xiang,[d] Sheshanath V. Bhosale*[e] Jing-Liang Li,[a] Richard A. Evans,*[f] and Akhil Gupta*[a,1]

a Institute for Frontier Materials, Deakin University, Waurn Ponds, Victoria 3216 Australia; Tel: +61 402 131 118; orcid.org/0000-0002-1257-8104

[1] **Current Address (A.G.)**: ARC Centre of Excellence in Exciton Science, School of Chemistry, Bio21 Institute, University of Melbourne, 30 Flemington Road, Parkville, Victoria 3010, Australia; E-mail: akhil.gupta1@unimelb.edu.au; Tel: +61 402 131 118; orcid.org/0000-0002-1257-8104

[b] School of Science, RMIT University, GPO Box 2476, Melbourne, Victoria 3001, Australia

[c] Molecular and Materials Modelling, Data61 CSIRO, Docklands, Victoria 8012, Australia

[d] State Key Laboratory of Silicate Materials for Architectures, Wuhan University of Technology, 122 Luoshi Rd, Wuhan 430070, Hubei, P. R. China

[e] Department of Chemistry, Goa University, Taleigao Plateau, Goa 403206, India; Email: svbhosale@unigoa.ac.in; Tel: +91 (0866) 9609303; orid.org/0000-0003-0979-8250

[f] CSIRO Manufacturing, Bayview Avenue, Clayton South, Victoria 3169 Australia; E-mail: richard.evans@csiro.au; Tel: +61 3 9545 2507.

Abstract

Through the direct connection of the donor nitrogen atom to oligothiophenes, herein we report three novel, donor materials for evaluation in bulk-heterojunction solar cells. The direct substitution enhances the charge transfer transition, thus improving the light-harvesting ability of the target chromophores. The influence of various terminal acceptor functionalities on the optoelectronic and photovoltaic properties was systematically studied. The target chromophore, **T3**, bearing oxoindenemalononitrile acceptor unit afforded a power conversion efficiency of 6.12% when paired with the conventional acceptor, $PC_{61}BM$, a result that is the highest in the current literature for push-pull chromophores.

Keywords: Solution-processable; ditolylamino; oligothiophene; bulk-heterojunction, donor-acceptor

1. Introduction

The development of renewable energy technologies based on harvesting solar energy at an affordable price is a challenging demand for society. The technologies such as solution-processed bulk heterojunction (BHJ) organic solar cells and dye-sensitized solar cells are highly promising [1–4], and the former in particular where it has attracted significant attention due to its notable merits such as low-cost, flexibility, ease of large-area fabrication by roll-to-roll printing and, above all, light weight [5]. The development of such BHJ devices has seen advancements in the areas of new material design and fabrication strategies. In terms of understanding material design, device morphology, charge transfer and consistent device outcome, a number of conventional donor and acceptor materials, for example donor polymer poly(3-hexyl thiophene) (P3HT) and soluble fullerene acceptors, [6,6]-phenyl-C_{61}-butyric acid methyl ester ($PC_{61}BM$) and its C_{71} analogue ($PC_{71}BM$), have been developed. These material combinations have been replaced with a number of alternate donors, for instance

conjugated polymers and small molecules, and acceptors, such as non-fullerene, in order to make the BHJ device technology viable for real-world applications [6–11].

It is evident from the current literature that in terms of material advancement, two types of donor materials, namely polymers and small molecules, have been developed for their application in BHJ devices. As far as acceptor materials are concerned, the fullerene derivatives act as excellent acceptor materials in organic photovoltaic (OPV) research, mainly due to their advantages such as good electron mobility (typically ranging 10^{-3}–10^{-4} cm^2 V^{-1} s^{-1}), excellent solubility and an ability to form a favourable nanoscale network with versatile donor semiconducting components [12–13]. Over the past few years, the power conversion efficiencies (PCEs) have displayed a rapid improvement with values surpassing 10% for both polymer- and small molecule-based OPV devices with fullerene derivatives as acceptors [14–17]. However, it is notable to mention that the use of small molecules instead of conjugated polymers has the potential to simplify synthesis and purification, and enable greater control over energy levels and device morphology [18–23]. Moreover, they can be considered as the candidates of choice for investigating the chemical structure-photovoltaic performance relationship, a crucial correlation whose understanding is paramount for future molecular designs to achieve higher and reproducible photovoltaic performance.

In their simplest form, small molecules for use in OPV devices consist of various fragments known as donor (D), acceptor (A) and a conjugated functionality known as π-spacer that typically connects these D and A units. The D and A units are also called as push and pull functionalities, respectively, and depending on the arrangement of these functionalities, a target material is labelled as e.g. D–A, A–D–A and D–A–D, to name a few. Even though the success of small molecule donors is noteworthy [2,6,24–27], incentives remain to develop materials that not only have better properties than the literature reported,

but will also have crucial characteristics such as solubility and energy levels complementing those of the conventional fullerene acceptors such as $PC_{61}BM$.

Given our particular interest in the development of D–A materials, and the fact that D–A design offers a straightforward path to insights into structure and performance relationships, we have demonstrated a strategy where the donor amine nitrogen is a direct substituent on the oligothiophene spacer, thus, avoiding the hindering or throttling of charge transfer transition from push to pull unit due to the presence of a phenyl group [28]. The direct connection of heteroatom to the oligothiophenes has been advantageous for significant spectral red-shift and improved BHJ performance. In this report, we employ the same design to develop novel donor materials for OPV applications and have used a ditolylamino donor unit with the direct substitution of the amine nitrogen on oligothiophene. We have developed three donor materials where we have used different acceptor functionalities to provide tuning of optical and electronic properties. The examined acceptors were cyanoacetate, cyanopyridone and dicyanoindenedione that were used to generate targets 2-methoxyethyl (*E*)-2-cyano-3-(5''-(di-*p*-tolylamino)-[2,2':5',2''-terthiophen]-5-yl)acrylate (**T1**), (*E*)-5-((5''-(di-*p*-tolylamino)-[2,2':5',2''-terthiophen]-5-yl)methylene)-1-(2-ethylhexyl)-4-methyl-2,6-dioxo-1,2,5,6-tetrahydropyridine-3-carbonitrile (**T2**), and (*Z*)-2-(2-((5''-(di-*p*-tolylamino)-[2,2':5',2''-terthiophen]-5-yl)methylene)-3-oxo-2,3-dihydro-1*H*-inden-1-ylidene)malononitrile (**T3**), respectively (see Fig. 1). It was demonstrated that the intramolecular charge transfer (ICT) transition was enhanced with the use of an acceptor group with increased acceptor strength, which in-turn is responsible for greater light-harvesting and better positioning of energy levels. It was further demonstrated that the design of investigated targets was validated as the solution-processed BHJ devices based on the blend of **T3**: $PC_{61}BM$ (1:1 *w*/*w*) exhibited PCE as high as 6.12%, which in fact is the highest in the current literature for push-pull systems where there is a direct connection of a donor heteroatom to an oligothiophene. It

is noteworthy to mention that the present work is a continuation of our efforts made in the design and development of small molecule chromophores for OPV applications [29–32].

The newly designed materials **T1**, **T2** and **T3** were synthesised *via* the Knoevenagel condensation reaction of 5''-(di-*p*-tolylamino)-[2,2':5',2''-terthiophene]-5-carbaldehyde with active methylene groups of various acceptor groups and their chemical structures were confirmed by ^{1}H and ^{13}C NMR spectroscopies, and high-resolution mass spectrometry. All the materials were highly soluble in a variety of conventional organic solvents and were found to be thermally stable as was indicted by thermogravimetric analysis (TGA) (for TGA curves, see Fig. S1, Supplementary Information (SI)). Importantly, the high solubility of organic semiconducting materials is crucial for fabricating solution-processable BHJ devices, and **T1**, **T2** and **T3** fulfil this criterion.

Figure 1 here

2. Experimental details

2.1 Materials and methods

2.1.1 Materials

2-Methoxyethyl cyanoacetate was purchased from Sigma-Aldrich Co., Australia. Synthesis of 5''-(*N*,*N*-di-*p*-tolylamino)-2'',5'-bithiophene-2',5-bithiophene-2-carboxaldehyde, cyanopyridone and dicyanoindenedione were reported previously [20,28,29].

2.1.2 General details

All the reactions were performed under an inert atmosphere of anhydrous nitrogen gas unless otherwise stated. Solvents used for various reactions were dried using a commercial solvent purification system. Solvents used in reaction extractions and chromatography, and all other reagents were used as supplied by commercial vendors without further purifications or drying. Thin layer chromatography (TLC) was performed using 0.25 mm thick plates pre-coated with silica gel (40−60 μm, F_{254}) and visualized using UV light (254 and 365 nm). Petroleum spirit with a boiling point range of 40−60 °C was used wherever indicated. Column chromatography was performed on either 40−60 or 20−40 μm silica gel. ^{1}H NMR spectra were recorded at 300, 400 or 500 MHz as indicated. The following abbreviations were used to explain multiplicities: s = singlet, d = doublet, t = triplet, q = quartet, m = multiplet, br = broad, dd = doublet of doublets, and dt = doublet of triplets. ^{13}C NMR spectra were recorded at 75, 101 or 125 MHz as indicated. ^{1}H and ^{13}C chemical shifts were calibrated using residual non-deuterated solvent as an internal reference and are reported in parts per million (δ) relative to tetramethylsilane (δ = 0). IR-Spectra were recorded on Thermo Nicolet Nexus 670 spectrometer in the form of non-hygroscopic KBr pellets. For high-resolution mass spectra (HRMS), atmospheric-pressure chemical ionization (APCI) experiments were carried out on FTMS, ionizing by APCI from an atmospheric solids analysis probe (ASAP). TGA experiments were carried out using Q-500 TGA instrument with nitrogen as a purging gas. Samples were heated to 800 °C at a rate of 10 °C/minute under nitrogen atmosphere. UV–Vis absorption spectra were recorded using a Hewlett Packard HP 8453 diode array spectrometer. PESA measurements were recorded using a Riken Keiki AC-2 PESA spectrometer with a power setting of 5 nW and a power number of 0.5. Samples for PESA were prepared on cleaned glass substrates. Electrochemical measurements were carried out using a PowerLab ML160 potentiostat interfaced via a PowerLab 4/20 controller to a PC

running E-Chem For Windows version 1.5.2. The measurements were run in argon-purged dichloromethane with tetrabutylammonium hexafluorophosphate (0.1 M) as the supporting electrolyte. The cyclic voltammograms were recorded using a standard three electrode configuration with a glassy carbon (2 mm diameter) working electrode, a platinum wire counter electrode and a silver wire pseudo reference electrode. The silver wire was cleaned in concentrated nitric acid followed by concentrated

hydrochloric acid and then washed with deionised water. Cyclic-voltammograms were recorded with a sweep rate of 50 mV s^{-1}. All the potentials were referred to the $E_{1/2}$ of ferrocene/

ferrocenium redox couple. Atomic force microscopy (AFM) topographic maps were directly performed on the active layers of the **T1**/**T2**/**T3**: $PC_{61}BM$ blends using an Asylum Research MFP-3D-SA instrument. The AFM was run in intermittent contact mode (tapping mode) using MicroMasch NSC18 tips (typical resonant frequency ~100 kHz, typical probe radius ~10 nm and typical aspect ratio 3: 1). A Bruker AXS D8 Discover instrument with a general area detector diffraction system (GADDS) using Cu Kα source was utilized to obtain XRD patterns.

2.1.3 Device fabrication and characterization of photovoltaic devices

Indium tin oxide (ITO)-coated glass (Kintek, 15 Ω/□) was cleaned by standing in a stirred solution of 5% (*v*/*v*) Deconex 12PA detergent at 90 °C for 20 min. The ITO-coated glass was then successively sonicated for 10 min each in distilled water, acetone and isopropanol. The substrates were then exposed to a UV–ozone clean at room temperature for 10 min. UV/ozone cleaning of glass substrates was performed using a Novascan PDS-UVT, UV/ozone cleaner with the platform set to maximum height. The intensity of the lamp was greater than 36 mW/cm^2 at a distance of 10 cm. At ambient conditions the ozone output of the UV cleaner is greater than 50 ppm. Aqueous solutions of PEDOT/PSS (HC Starck,

Baytron P AI 4083) were filtered (0.2 µm RC filter) and deposited onto glass substrates in air by spin coating (Laurell WS-400B-6NPP lite single wafer spin processor) at 5000 rpm for 60 s to give a layer having a

thickness of 40 ± 5 nm. The PEDOT/PSS layer was then annealed on a hotplate in a glove box at 145 °C for 10 min. For OPV devices, the newly synthesized organic *p*-type materials and $PC_{61}BM$ (Nano-C) were dissolved in individual vials by magnetic stirring. Blend ratios and solution concentrations were varied to optimize device performance. The solutions were then combined, filtered (0.2 µm RC filter) and deposited by spin coating onto the ITO-coated glass

substrates inside a glove box. The coated substrates were then transferred (without exposure to air) to a vacuum evaporator inside an adjacent nitrogen-filled glove box. Samples were placed on a shadow mask in a tray. The area defined by the shadow mask gave device areas of exactly 0.2 cm^2. Deposition rates and film thicknesses were monitored using a calibrated quartz thickness monitor inside the vacuum chamber. Layers of calcium (Ca) (Aldrich) and aluminium (Al) (3 pellets of 99.999%, KJ Lesker) having thicknesses of 20 nm and 100 nm, respectively, were evaporated from open tungsten boats onto the active layer by thermal evaporation at

pressures less than 2×10^{-6} mbar. A connection point for the ITO electrode was made by manually scratching off a small area of the active layers. A small amount of silver paint (Silver Print II, GC Electronics, part no.: 22-023) was then deposited onto all of the connection points, both ITO and Al. The completed devices were then encapsulated with glass and a UV-cured epoxy (Summers Optical, Lens Bond type J-91) by exposing to 365 nm UV light inside a glove box for 10 min. The encapsulated devices were then removed from the glove box and tested in air within 1 h. The OPV devices were tested using an Oriel solar simulator fitted with a 1000 W xenon lamp filtered to give an output of 100 mW/cm^2 at

simulated AM 1.5. The lamp was calibrated using a standard, filtered silicon (Si) cell from Peccell Limited which was subsequently cross-calibrated with a standard reference cell traceable to the National Renewable Energy Laboratory. The devices were tested using a Keithley 2400 Sourcemeter controlled by labview software. Film thicknesses were determined using a Dektak 6M Profilometer.

2.2 Synthetic details

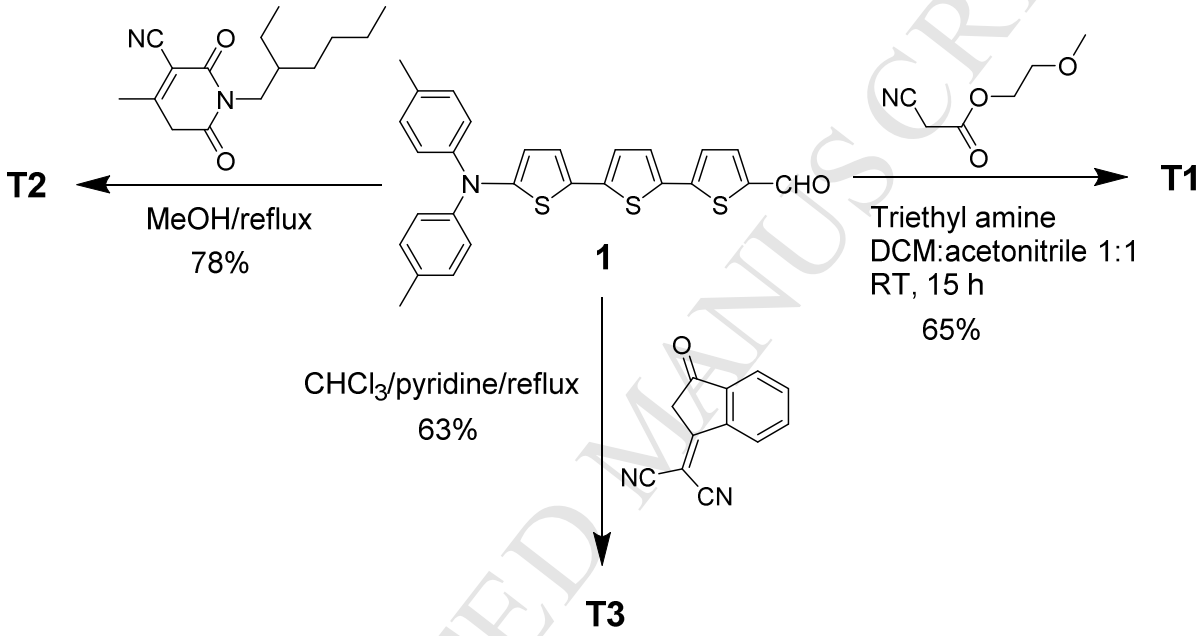

Scheme 1 The synthetic protocol used to synthesize **T1**, **T2** and **T3**.

2.2.1 2-Methoxyethyl (E)-2-cyano-3-(5''-(di-p-tolylamino)-[2,2':5',2''-terthiophen]-5-yl)acrylate (**T1**): The synthesis of **T1** was carried out in a similar manner as was reported previously [30]. Cherry solid; M. Pt.: 151–154 °C; IR (cm^{-1}) 3032, 2923, 2216, 1720, 1649, 1584, 1509, 1430, 1373, 1265, 1205, 818; δ_H (400 MHz, CD_2Cl_2) 8.26 (1H, s), 7.68–7.67 (1H, m), 7.30–7.29 (1H, m), 7.24–7.23 (1H, m), 7.12–7.05 (8H, m), 7.01–7.00 (1H, m), 6.97–6.95 (1H, m), 6.46–6.42 (1H, m), 4.42–4.39 (2H, m), 3.69–3.66 (2H, m), 3.39 (3H, s), 2.31 (6H, s); δ_C (400 MHz, CD_2Cl_2) 162.9, 153.5, 146.2, 145.0, 139.7, 133.7, 129.8, 127.5, 123.9,

123.7, 123.4, 123.2, 117.7, 116.0, 96.9, 70.1, 65.3, 58.8, 20.5; HRMS (APCI): $[M+H]^+$, found 597.1338. $C_{33}H_{29}N_2O_3{}^{32}S_3$ requires 597.1335.

2.2.2 (E)-5-((5''-(di-p-tolylamino)-[2,2':5',2''-terthiophen]-5-yl)methylene)-1-(2-ethylhexyl)-4-methyl-2,6-dioxo-1,2,5,6-tetrahydropyridine-3-carbonitrile (**T2**): The synthesis of **T2** was done in an identical manner as was reported previously [20]. Black solid; M. Pt.: 182–185 °C; IR (cm^{-1}) 2956, 2925, 2857, 2217, 1682, 1634, 1544, 1507, 1421, 1378, 1296; δ_H (400 MHz, $CDCl_3$) 7.82 (1H, s), 7.65–7.64 (1H, m), 7.41–7.40 (1H, m), 7.28–7.27 (1H, m), 7.11–7.06 (8H, m), 6.99–6.98 (1H, m), 6.96–6.95 (1H, m), 6.44–6.43 (1H, m), 3.98–3.88 (2H, m), 2.59 (3H, s), 2.31 (6H, s), 1.89-1.82 (1H, m), 1.39-1.19 (8H, m), 0.91–0.86 (6H, m); δ_C (400 MHz, $CDCl_3$) 163.3, 161.0, 158.0, 154.4, 154.0, 146.9, 144.9, 143.8, 141.9, 135.9, 133.8, 133.2, 129.9, 128.4, 126.9, 124.3, 124.1, 123.6, 123.4, 117.3, 115.6, 115.2, 103.2, 43.9, 37.4, 30.5, 28.4, 23.8, 23.1, 20.8, 18.9, 14.2, 10.6; HRMS (APCI): $[M+H]^+$, found 716.2426. $C_{42}H_{42}N_3O_2{}^{32}S_3$ requires 716.2434.

2.2.3 (Z)-2-(2-((5''-(di-p-tolylamino)-[2,2':5',2''-terthiophen]-5-yl)methylene)-3-oxo-2,3-dihydro-1H-inden-1-ylidene)malononitrile (**T3**): Synthesis of **T3** was done adopting a similar method reported previously [29]. Black solid with metallic lustre; M. Pt.: 218–221 °C; IR (cm^{-1}) 3065, 3027, 2920, 2859, 2217, 1699, 1559, 1542, 1507, 1425, 1385, 1317, 1218, 1134, 1046; δ_H (400 MHz, $CDCl_3$) 8.80 (1H, s), 8.67–8.64 (1H, m), 7.91–7.88 (1H, m), 7.76–7.69 (3H, m), 7.39–7.38 (1H, m), 7.25–7.24 (1H, m), 7.25 (3H, s), 7.14–7.05 (5H, m), 7.03–6.96 (2H, m), 6.44–6.43 (1H, m), 2.32 (6H, s); δ_C (400 MHz, $CDCl_3$) 188.59, 160.57, 154.22, 153.89, 146.68, 145.09, 142.22, 140.17, 137.67, 137.01, 135.68, 135.23, 134.56, 133.95, 133.32, 130.15, 128.54, 127.09, 125.41, 124.56, 124.32, 123.85, 123.76, 123.62, 121.85, 117.48, 114.86, 114.79, 69.23, 21.03; HRMS (APCI): $[M+H]^+$, found 648.1231. $C_{39}H_{26}N_3O^{32}S_3$ requires 648.1233.

3. Results and discussion

3.1. Optical and electrochemical properties

The ultraviolet–visible (UV–Vis) spectral absorptivities of all the materials were measured in chloroform solution and are represented in Fig. 2. The longest wavelength absorption maximum (λ_{max}) exhibited by **T1** was at 503 nm, whereas **T2** and **T3** exhibited their maxima at 603 nm and 653 nm, respectively. As predicted, both the absorption maximum and extinction coefficient increased with increasing acceptor strength, i.e. λ_{max} (**T1**) < λ_{max} (**T2**) < λ_{max} (**T3**) and ε (= 41,120 L Mol^{-1} cm^{-1}; **T1**) < ε (= 59,570 L Mol^{-1} cm^{-1}; **T2**) < ε (= 78,960 L Mol^{-1} cm^{-1}; **T3**). The stronger acceptor group, dicyanoindenedione, induced a significant red-shift in the absorption of compound **T3** such that the absorption tails into the near-infrared region. This enhanced profile allows a larger amount of the solar spectrum to be absorbed. With increased acceptor strength, we found a 33% enhancement to the peak molar absorptivity of compound **T3** compared with compound **T2**, which itself showed an improvement of 45% when compared with **T1**. Of particular relevance, we observe the same bathochromic absorption shift in thin film spectra of compounds **T3**, **T2** and **T1**. The bathochromic shift in absorbance maxima of thin films is clearly shown in Fig. 2.

To understand the distribution of the highest occupied molecular orbital (HOMO) and the lowest unoccupied molecular orbital (LUMO) densities, we performed density functional theory (DFT) calculations on all the materials using the Gaussian 09 suite of programs and the B3LYP/6-311+G(d,p)//B3LYP/6-31G(d) level of theory [33]. DFT calculations indicated the effect on the LUMO energy level as we change the acceptor units. The HOMO densities were evenly distributed on the molecular backbone, whereas the LUMO densities were mainly localised on the acceptor parts (Fig. 3). It was observed that as the acceptor strength grows, the LUMO density was tightly held by that particular acceptor unit. The distribution of the HOMO and the LUMO densities indicated that the HOMO → LUMO excitation shifts

the electron flow from the phenyl amino unit (donor fragment) to the corresponding acceptor functionality.

Figure 2 here

Figure 3 here

Experimentally, the HOMO energies of **T1**, **T2** and **T3** were estimated using photo electron spectroscopy in air (PESA). The PESA measurements were performed on thin solid films to measure work functions which correspond to the HOMO values (for PESA curves, see Fig. S2, SI). The LUMO energies were calculated by adding the bandgap to the HOMO values. The LUMO energy level of **T3** was reduced by 0.12 eV in comparison to **T2**, which in fact was lessened by 0.32 eV when compared with **T1**. These experimental findings followed the theoretical pattern, which indicated that as the acceptor strength increases, band gap decreases. Furthermore, the electrochemistry experiments revealed that all of materials undergo reversible oxidation processes on the anodic sweep, whereas indicated irreversible cycles on the cathodic sweep [34,35]. The former in particular suggests the suitability of **T1**, **T2** and **T3** as *p*-type materials in BHJ devices (see Fig. 4 for cyclic voltammogram curves). The measurement of the HOMO energy levels using cyclic voltammetry (CV) followed the similar trend as was established using PESA experiments. These experimental estimations of the HOMO and the LUMO energies using PESA and CV indicated that the band gaps of these materials are all in the range required of donor materials for BHJ devices and are significantly narrower in magnitude than 2.0 eV measured for P3HT. Fig. 5 shows the alignment of various energy levels measured on as-casted thin films of **T1**, **T2** and **T3**, and Table 1 indicates comparative optoelectronic properties.

Figure 4 here

Figure 5 here

Table 1. Comparative optoelectronic properties of **T1**, **T2** and **T3**

Dye	Absorption (solution) λ_{max}[a]/nm [ε/(Lt M^{-1} cm^{-1})]	Absorption (film) λ_{max}[b]/onset/nm	E_{HOMO} eV[c] (Th. value) (CV value)[f]	$E_{bandgap}$ eV[d] (Th. value) (CV value)[f]	E_{LUMO} eV[e] (Th. value) (CV value)[f]
T1	523 [41, 120]	536/670	-5.31 (-5.22) (-5.16)	1.85 (2.20) (1.87)	-3.46 (-3.02) (-3.29)
T2	603 [59, 570]	635/860	-5.22 (-5.35) (-5.11)	1.44 (1.98) (1.55)	-3.78 (-3.37) (-3.56)
T3	653 [78, 960]	677/920	-5.25 (-5.26) (-5.05)	1.35 (1.86) (1.46)	-3.90 (-3.40) (-3.59)

a Absorption spectra were measured in chloroform solution. b Absorption spectra of thin

solid films spin-casted from chloroform solutions. c The HOMO levels of the dyes were measured using PESA on thin solid films which were casted on cleaned glass substrates. d Energy band gaps were estimated from the tangent of the edge of the longest wavelength in thin solid films. e The LUMO levels were calculated from the optical band gaps (film) and HOMO levels ($E_{LUMO}= E_{bandgap}+ E_{HOMO}$)

f Values using cyclic voltammograms

3.2. Photovoltaic properties

Having established that newly developed materials possess potential optoelectronic properties, adequate solubility and thermal stability, we evaluated their performance as donor materials (*p*-type) with the soluble fullerene derivative $PC_{61}BM$ as the *n*-type semiconductor in solution-processable BHJ devices under simulated sunlight and monochromatic light illumination. We planned a very simple device architecture to commence with and to observe initial performance, stability and device fabrication conditions. For all the compounds the device structure used was ITO/PEDOT: PSS (38 nm)/active layer/Ca (20 nm)/Al (100 nm) where the active layer was a solution-processed blend of either of **T1**, **T2** and **T3** and the solubilized fullerene derivative ($PC_{61}BM$). For **T1**, an optimised PCE of 4.53% was achieved when the active layer was spin-coated from a chlorobenzene solution as a 1:1 blend. By contrast, the maximum PCEs obtained for the devices based on **T2** and **T3** were 4.82% and 6.12%, respectively, when spun under similar conditions. The recorded PCE (>6%) is among the highest efficiencies obtained by a single junction BHJ device based on the combination of an unthrottled push-pull donor target and the conventional fullerene acceptor. The current–voltage curves for the optimised blends of **T1**, **T2** and **T3** together with the conventional combination of P3HT: $PC_{61}BM$ are depicted in Fig. 6 (see Table 2 for detailed device parameters).

Figure 6 here

Table 2. Photovoltaic cell parameters for **T1**, **T2** and **T3** blends

Donor	**Acceptor**	**Testing conditions (donor: acceptor)[a]**	V_{oc} **(V)**	J_{sc} **(mA/cm^2)**	***FF***	**Best PCE (%)**	**Average PCE (%) (± std dev)**
T1	$PC_{61}BM$	1: 1	0.93	8.42	0.57	4.53	4.42 (± 0.09)
T2	$PC_{61}BM$	1: 1	0.84	9.31	0.61	4.82	4.71 (± 0.08)
T3	$PC_{61}BM$	1: 1	0.88	11.02	0.63	6.12	6.02 (± 0.06)
P3HT	$PC_{61}BM$	1: 1[b]	0.57	8.28	0.64	3.02	2.95 (± 0.05)

[a] BHJ devices with specified weight ratio. Device structure was ITO/PEDOT: PSS (38 nm)/active layer/Ca (20 nm)/Al (100 nm) with an active layer thickness of ~65 nm

[b] A standard P3HT: $PC_{61}BM$ device afforded 3.02% efficiency when tested under alike conditions

The incident photon-to-current conversion efficiency (IPCE) spectra of the blended films with a D/A weight ratio of 1:1 are shown in Fig. 7. For **T1**, the IPCE shows a maximum of ~40% at 510 nm whereas for **T2** and **T3**, the IPCE maxima were 48% and 57% at 535 nm and 740 nm, respectively. The blended films showed broad IPCE spectra ranging from 350 to 1000 nm, typically over most of the visible region, and in particular for **T3** where the IPCE spectrum tails into the near infra-red region. The higher and broader peak IPCE together with the superior device performance in case of **T3** can be attributed to strong light-harvesting and the use of an acceptor unit with greater accepting strength when compared with other acceptor units used in **T1** and **T2**. These IPCE spectra matched the blend film absorption profiles and the broadness of these spectra indicated that both donor and acceptor components in active blends made a considerable contribution to the IPCE and J_{sc} (for blend absorption spectra, see Fig. S3, SI). Furthermore, the photocurrents obtained from the IPCE data were in close agreement with those of the current–voltage measurements conducted under the one Sun conditions. The physical observance of the blend films indicated the high-quality intermixing of donor and acceptor domains, and **T3** in particular, and encouraged us to perform atomic force microscopy (AFM) analysis which was conducted in tapping mode. The AFM analysis indicated that the surface roughnesses were low in order (**T1** = 4.7 nm, **T2** = 5.8 and **T3** = 3.9 nm), a result that corroborated our physical observation. The **T3**: $PC_{61}BM$ blend in particular showed superior morphology with better phase separation, a finding that is advantageous to higher device outcome. Such a well-plaited surface (**T3**: $PC_{61}BM$ blend) was further confirmed by transmission electron microscopy (TEM) analysis where we were able to observe a finer texture when compared with analogous blend surfaces (**T1** and **T2**). Such smoother and featureless surfaces usually result in relatively higher values of J_{sc} and *FF* as is the case of **T3**. The AFM and TEM images of all the blend surfaces are shown in Figs. 8 and 9, respectively. Furthermore, in order to observe blend surface crystallinity, if any, we

conducted X-ray diffraction (XRD) analysis. We found all the blend surfaces to be amorphous, thus eliminating the probability of morphologies such as granular (for XRD spectra, see Fig. S4, SI). However, the AFM, TEM and XRD analyses did suggest that it was target materials' greater ability to intermix with the acceptor component that was an important contribution to the observed device performance. To gain insight into the effective charge carrier mobilities, the space charge limited current (SCLC) method was applied to get information about the charge transportation in the devices. The hole-only devices, consisting of active layer sandwiched between a PEDOT: PSS coated ITO substrate and a MoO_3/Ag counter-electrode, were fabricated as per the sketch depicted in Fig. S5, SI. From the current density as a function of voltage data curve, the hole mobility in the SCLC region can be estimated using the Mott-Gurney equation, [($J = 9/8(\varepsilon_0\varepsilon_r\mu)\ (V^2/d^3)$], where J is the current density, $V = V_{appl}$-V_{bi} (V_{appl} is the applied potential and V_{bi} is the built-in potential resulting from work function difference between two electrodes), ε_r is the dielectric constant of the donor material, ε_0 is the permittivity of vacuum, μ is the hole mobility, and d is the donor materials' (**T1**/**T2**/**T3**) film thickness. Using this expression, good hole mobilities ranging $10^{-4} - 10^{-5}$ $cm^2\ V^{-1}\ s^{-1}$ were observed which is certainly beneficial for achieving higher J_{sc} and *FF* values with the resulting OPV devices (Fig. S5, SI). From the hole mobility experiment, one can see that the hole mobility of **T2** is slightly higher than **T3**, though the order of mobility is same. However, it is well understood that the hole mobility itself is not a prime factor for any material to give higher performance. Given the comparison of two structural analogues, there are a number of factors that are responsible and to be considered for better OPV performance. One such factor is the blend film morphology and the other being the miscibility of donor and acceptor domains. In the present study, the miscibility and surface characteristics of **T3** as a donor domain are way better than **T2** when blended with its acceptor counterpart, thus, giving better performance than **T2**. For a clear understanding, the

AFM and TEM images can be referred. The reasonable hole mobilities further underline the utility of the design concepts used in **T1**, **T2** and **T3**.

Figure 7 here

Figure 8 here

Figure 9 here

4. Conclusions

In summary, we have demonstrated the utilization of the direct connection of donor amine (nitrogen atom) to oligothiophenes for generating donor–acceptor small molecules, **T1**, **T2** and **T3**, in OPV applications. Our idea of designing **T1**, **T2** and **T3** by increasing the range of acceptor strengths was clearly justified as the solution-processable BHJ devices afforded very encouraging and reasonable outcome, for instance **T3**:$PC_{61}BM$ 1:1 = 6.12%. Not only are **T1**, **T2** and **T3** the first reported examples in the literature where unthrottled design in-conjunction with wide-ranging acceptor groups have been explored for OPV applications, but the device outcome reported herein is among the highest efficiencies that has been achieved using a simple device architecture and for the investigated class of push-pull oligothiophene chromophores.

Acknowledgements

A. G. acknowledges Dr Gerry Wilson from CSIRO Manufacturing, Clayton, Victoria, Australia, for providing support through a visiting fellow position. A. G. would like to thank Australia India Institute (AII), New Delhi, India for providing an Incoming Leader Fellowship Award that enabled him to carry out this very interesting piece of research and also for supporting him with the necessary requirements for this project. A. A., A. K. H., A. G. and J. C. acknowledge the fabrication and analytical facilities at Deakin, Wuhan and RMIT Universities. J. Li acknowledges the Australian Research Council (ARC) for support through a Future Fellowship project (FT130100057). S. V. B. acknowledges University Grant Commission (UGC) – Faculty Research Program (India) – for providing financial support and an award of professorship.

References

[1] Huang Y, Kramer EJ, Heeger AJ, Bazan GC. Bulk heterojunction solar cells: morphology and performance relationships. Chem Rev 2014;114:7006–47.

[2] Lin Y, Li Y, Zhan X. Small molecule semiconductors for high-efficiency organic photovoltaics. Chem Soc Rev 2012;41:4245–72.

[3] Rananaware A, Gupta A, Li J-L, Bilic A, Jones L, Bhargava S, Bhosale SV. A four-directional non-fullerene acceptor based on tetraphenylethylene and diketopyrrolopyrrole functionalities for efficient photovoltaic devices with a high open-circuit voltage of 1.18 V. Chem Commun 2016;52:8522–25.

[4] Xiang W, Gupta A, Kashif MK, Duffy N, Bilic A, Evans RA, et al. Cyanomethylbenzoic acid: an acceptor for donor–π–acceptor chromophores used in dye-sensitized solar cells. ChemSusChem 2013;6:256–60.

[5] Service RF. Outlook brightens for plastic solar cells. Science 2011;332:293.

[6] Mishra A, Bäuerle P. Small molecule organic semiconductors on the move: promises for future solar energy technology. Angew Chem Int Ed 2012;51:2020–67.

[7] Li Y. Molecular design of photovoltaic materials for polymer solar cells: toward suitable electronic energy levels and broad absorption. Acc Chem Res 2012;45:723–33.

[8] Hangarge RV, Gupta A, Raynor AM, La DD, Bilic A, Li J-L, et al. Enhancing the efficiency of solution-processable bulk-heterojunction devices via a three-dimensional molecular architecture comprising triphenylamine and cyanopyridone. Dyes Pigm 2017;137:126–134.

[9] Lin Y, Zhan X. Non-fullerene acceptors for organic photovoltaics: an emerging horizon. Mater Horiz 2014;1:470–88.

[10] Gupta A, Rananaware A, Rao PS, La DD, Bilic A, Xiang W, et al. An H-shaped, small molecular non-fullerene acceptor for efficient organic solar cells with an impressive open-circuit voltage of 1.17 V. Mater Chem Front 2017;1:1600–06.

[11] Rananaware A, Gupta A, Kadam G, La DD, Bilic A, Xiang W, et al. Cyanopyridone flanked the tetraphenylethylene to generate an efficient, three-dimensional small molecule non-fullerene electron acceptor. Mater Chem Front 2017; 1:2511–8.

[12] He YJ, Chen HY, Hou JH, Li YF. Indene−C_{60} bisadduct: a new acceptor for high-performance polymer solar cells. J Am Chem Soc 2010;132:1377–82.

[13] Cheng YJ, Liao MH, Chnag CY, Kao WS, Wu CE, Hsu CS. Di(4-methylphenyl)methano-C_{60} bis-adduct for efficient and stable organic photovoltaics with enhanced open-circuit voltage. Chem Mater 2011;23:4056–62.

[14] Deng D, Zhang Y, Zhang J, Wang Z, Zhu L, Fang J, et al. Fluorination-enabled optimal morphology leads to over 11% efficiency for inverted small-molecule organic solar cells. Nat Commun 2016;7:13740.

[15] Wang J-L, Liu K-K, Yan J, Wu Z, Liu F, Xiao F, et al. Series of multifluorine substituted oligomers for organic solar cells with efficiency over 9% and fill factor of 0.77 by combination thermal and solvent vapor annealing. J Am Chem Soc 2016;38:7687–97.

[16] Zhao J, Li Y, Yang G, Jiang K, Lin H, Ade H, Ma W, Yan H. Efficient organic solar cells processed from hydrocarbon solvents. Nat Energy 2016;1:15027.

[17] Srivani D, Gupta A, Bhosale SV, Ohkubo K, Bhosale RS, Fukuzumi S, Bilic A, Jones LA, Bhosale SV. A triphenylamine–naphthalenediimide–fullerene triad: synthesis, photoinduced charge separation and solution-processable bulk heterojunction solar cells. Asian J Org Chem 2018;7:220–6.

[18] Kronenberg NM, Deppisch M, Würthner F, Lademann HWA, Deing K, Meerholz K. Bulk heterojunction organic solar cells based on merocyanine colorants. Chem Commun 2008;6489–91.

[19] Tamayo AB, Dang XD, Walker B, Seo J, Kent T, Nguyen TQ. A low band gap, solution processable oligothiophene with a dialkylated diketopyrrolopyrrole chromophore for use in bulk heterojunction solar cells. Appl Phys Lett 2009;94:103301.

[20] Gupta A, Ali A, Bilic A, Gao M, Hegedus K, Singh B, et al. Absorption enhancement of oligothiophene dyes through the use of a cyanopyridone acceptor group in solution-processed organic solar cells. Chem Commun 2012;48:1889–91.

[21] Sun H, Song X, Xie J, Sun P, Gu P, Liu C, Chen F, Zhang Q, Chen Z-K, Huang W. PDI derivative through fine-tuning the molecular structure for fullerene-free organic solar cells. ACS Appl Mater Interfaces 2017;9:29924–31.

[22] Chen W, Zhang Q. Recent progress in non-fullerene small molecule acceptors in organic solar cells (OSCs). J Mater Chem C, 2017;5:1275–1302.

[23] Chen W, Yang X, Long G, Wan X, Chen Y, Zhang Q. A perylene diimide (PDI)-based small molecule with tetrahedral configuration as a non-fullerene acceptor for organic solar cells. J Mater Chem C, 2015;3:4698–4705.

[24] Anthony JE. The larger acenes: versatile organic semiconductors. Angew Chem Int Ed 2008;47:452–83.

[25] Li Y, Guo Q, Li Z, Pei J, Tian W. Solution processable D–A small molecules for bulk-heterojunction solar cells. Energy Environ Sci 2010;3:1427–36.

[26] Gupta A, Ali A, Gao M, Singh B, Bilic A, Watkins SE, Bach U, Evans RA. Small molecules containing rigidified thiophenes and a cyanopyridone acceptor unit for solution-processable bulk-heterojunction solar cells. Dyes Pigm 2015;19:122–32.

[27] Bobe SR, Gupta A, Rananaware A, Bilic A, Bhosale SV, Bhosale SV. Improvement of optoelectronic and photovoltaic properties through the insertion of a naphthalene diimide unit in donor–acceptor oligothiophenes. RSC Adv 2015;5:4411–15.

[28] Gupta A, Armel V, Xiang W, Fanchini G, Watkins SE, Macfarlane DR, Bach U, Evans RA. The effect of direct amine substituted push–pull oligothiophene chromophores on dye-sensitized and bulk heterojunction solar cells performance. Tetrahedron 2013;69:3584–92.

[29] Gupta A, Ali A, Singh B, Bilic A, Bach U, Evans RA. Molecular engineering for panchromatic absorbing oligothiophene donor–π–acceptor organic semiconductors. Tetrahedron 2012;68:9440–47.

[30] Srivani D, Agarwal A, Bhosale SV, Puyad AL, Xiang W, Evans RA, Gupta A, Bhosale SV. Naphthalene diimide-based non-fullerene acceptors flanked by open-ended and aromatizable acceptor functionalities. Chem Commun 2017;53:11157–60.

[31] Rao PS, Gupta A, Bhosale SV, Bilic A, Xiang W, Evans RA, Bhosale SV. Donor–acceptor–acceptor-based non-fullerene acceptors comprising terminal chromen-2-one functionality for efficient bulk-heterojunction devices. Dyes Pigm 2017;146:502–11.

[32] Srivani D, Gupta A, Bhosale SV, Puyad AL, Xiang W, Li J-L, Evans RA, Bhosale SV. Non-fullerene acceptors based on central naphthalene diimide flanked by rhodanine or 1,3-indanedione. Chem Commun 2017;53:7080–3.

33 Frisch M, Trucks G, Schlegel H, Scuseria G, Robb M, Cheeseman J, et al. Gaussian 09, revision D. 01. Wallingford CT: Gaussian Inc; 2013.

[34] Wen S, Wang C, Ma P, Zhao Y-X, Li C, Ruan S. Synthesis and photovoltaic properties of dithieno[3,2-*b*:2′,3′-*d*]silole-based conjugated copolymers. J Mater Chem A, 2015;3:13794–800.

[35] Wen S, Pei J, Zhou Y, Li P, Xue L, Li Y, Xu B, Tian W. Synthesis of 4,7-diphenyl-2,1,3-benzothiadiazole-based copolymers and their photovoltaic applications. Macromolecules, 2009;42:4977–84.

[36] Yu P-P, Zhang, C-H, Chen L-L, Wei X-F, Lu Y-L, Luo D, Cao Y, Zhu X-H. Bis(dithienyldiketopyrrolopyrrole) compounds with a diethynylbithienyl linkage for organic solar cells. Dyes Pigm 2018;154:100–6.

[37] Xia Y, Tan W-Y, Wang L-P, Zhang C-H, Peng L, Zhu X-H, Peng J, Cao Y. Soluble acetylenic molecular glasses based on dithienyldiketopyrrolopyrrole for organic solar cells. Dyes Pigm 2016;126:96–103.

[38] Tan W-Y, Gao K, Zhang J, Chen L-L, Wu S-P, Jiang X-F, Peng X-B, Hu Q, Liu F, Wu H-B, Cao Y, Zhu X-H. Enhancing performances of solution-processed inverted ternary small-molecule organic solar cells: manipulating the host-guest donors and acceptor interaction. Solar RRL 2017;1:1600003–8.

LIST OF FIGURES

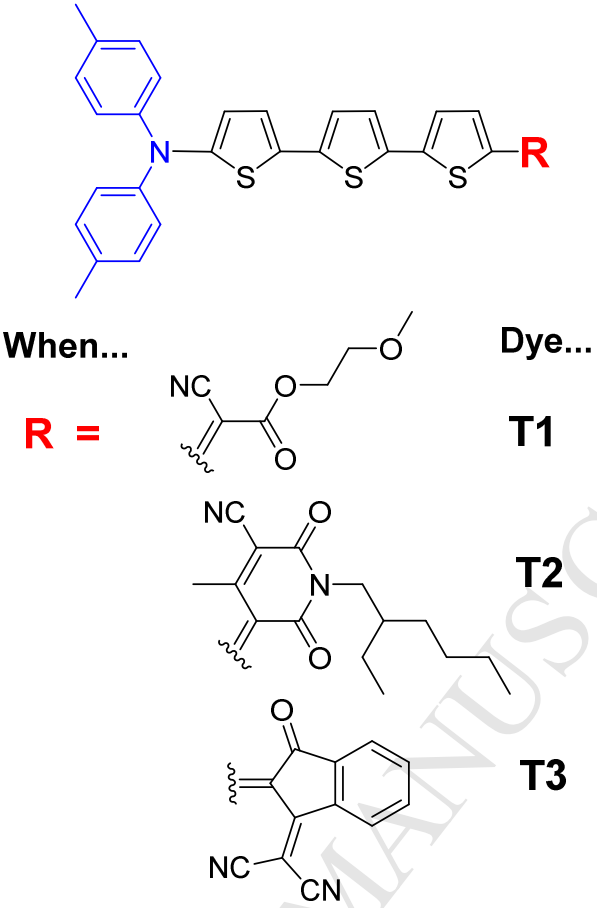

Fig. 1 Chemical structures of the newly designed materials investigated in the present study.

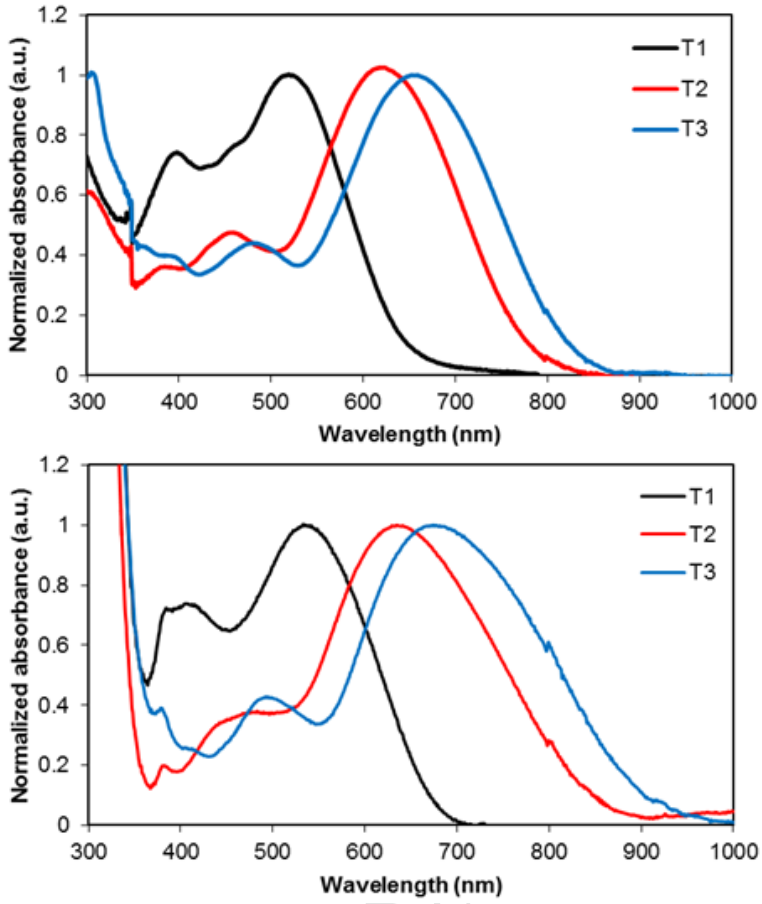

Fig. 2. Normalised UV–Vis absorption spectra of **T1**, **T2** and **T3** in chloroform solution (upper) and as thin solid films (lower).

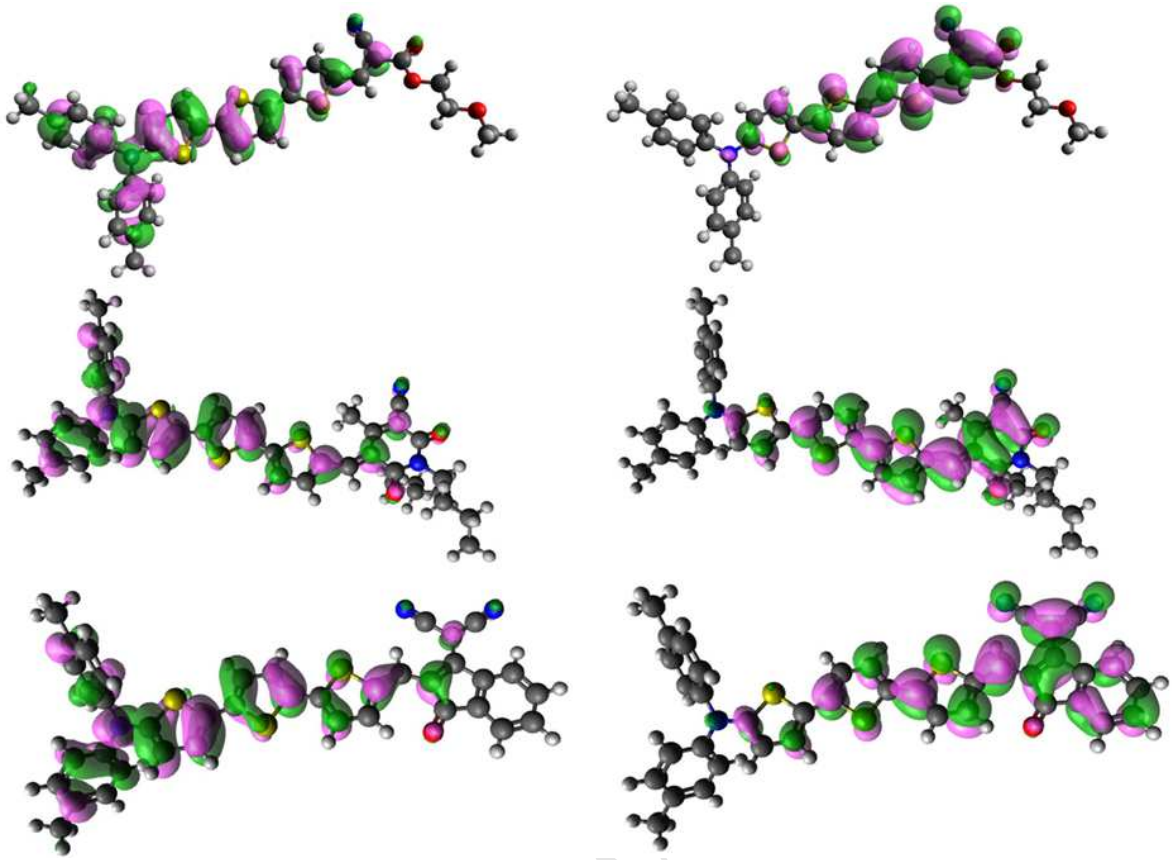

Fig. 3. Orbital density distribution for the frontier molecular orbitals of **T1** (upper), **T2** (middle) and **T3** (lower). Density functional theory calculations were performed using the Gaussian 09 suite of programs and the B3LYP/6-311+G(d,p)//B3LYP/6-31G(d) level of theory.

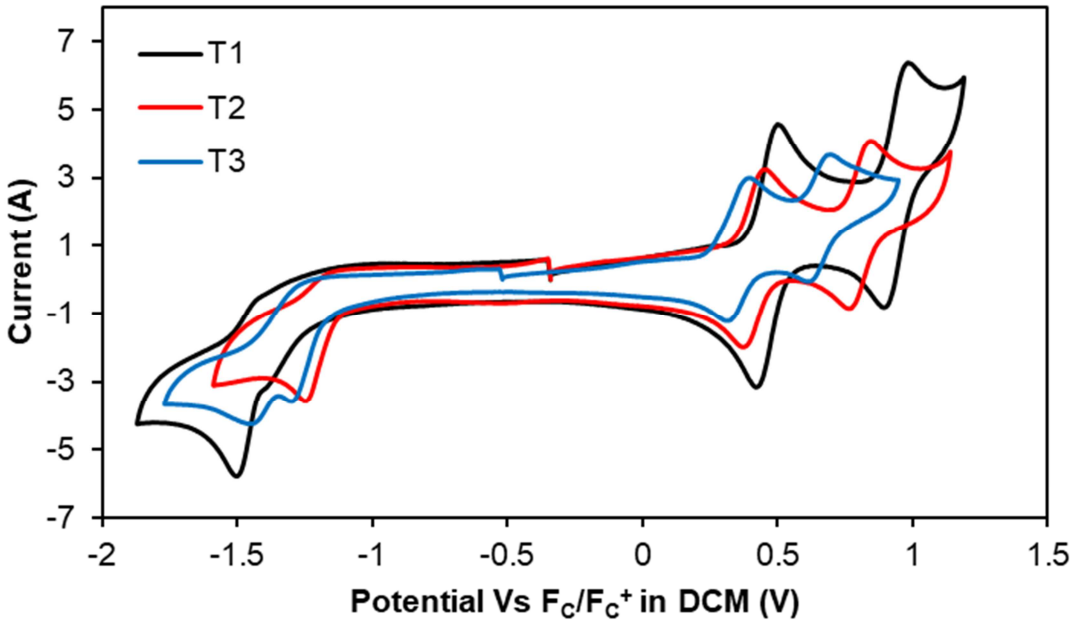

Fig. 4. Cyclic voltammograms of **T1**, **T2** and **T3** run in dichloromethane at a sweep rate of 50 mV s^{-1} showing reversible oxidation processes.

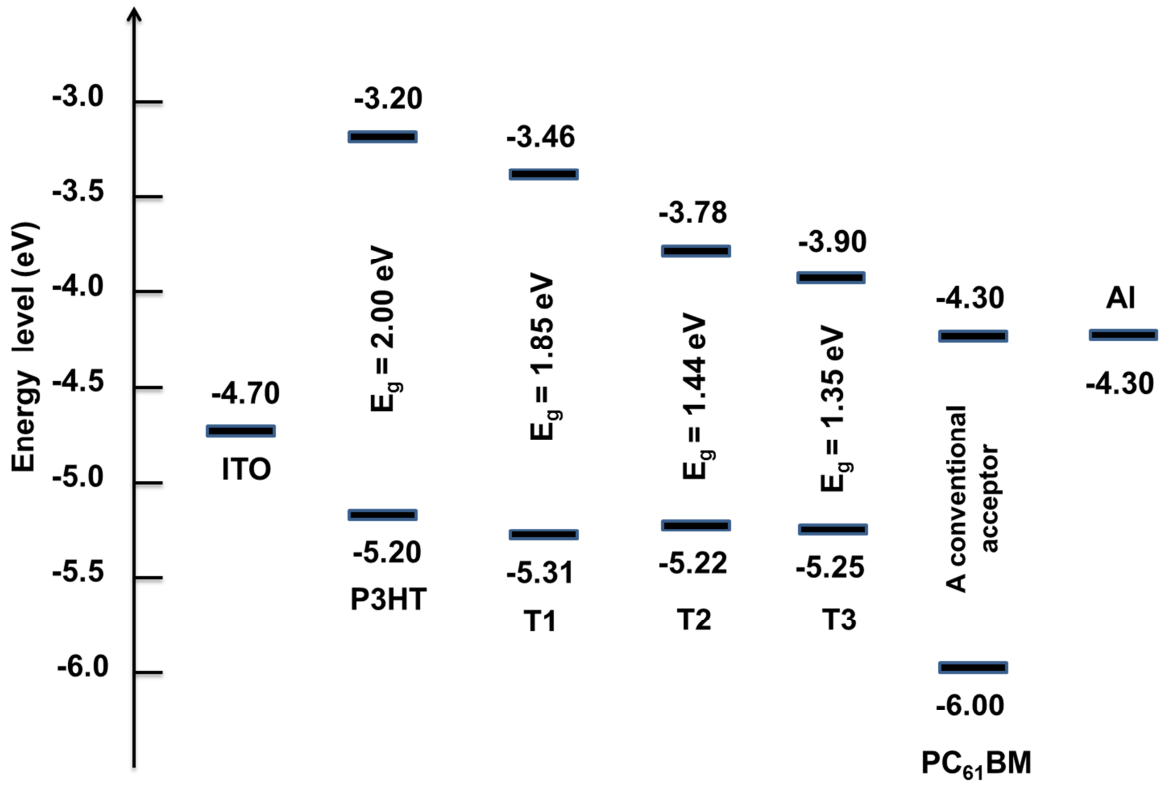

Fig. 5. The energy level diagram showing the alignment of various components of a BHJ device architecture.

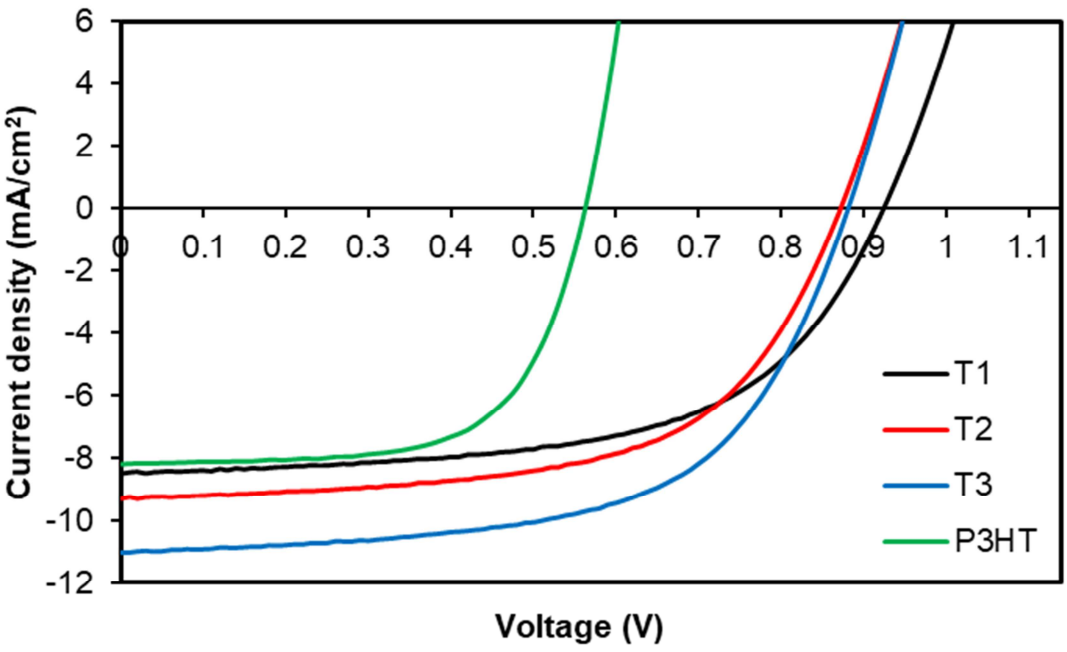

Fig. 6. Current–voltage curves for the optimised devices based on **T1**, **T2** and **T3** in blends with $PC_{61}BM$ (1:1 weight ratio) under simulated sunlight (100 mW cm^{-2} AM 1.5G). Device Structure is: ITO/PEDOT: PSS (38 nm)/active layer (~65 nm)/Ca (20 nm)/Al (100 nm).

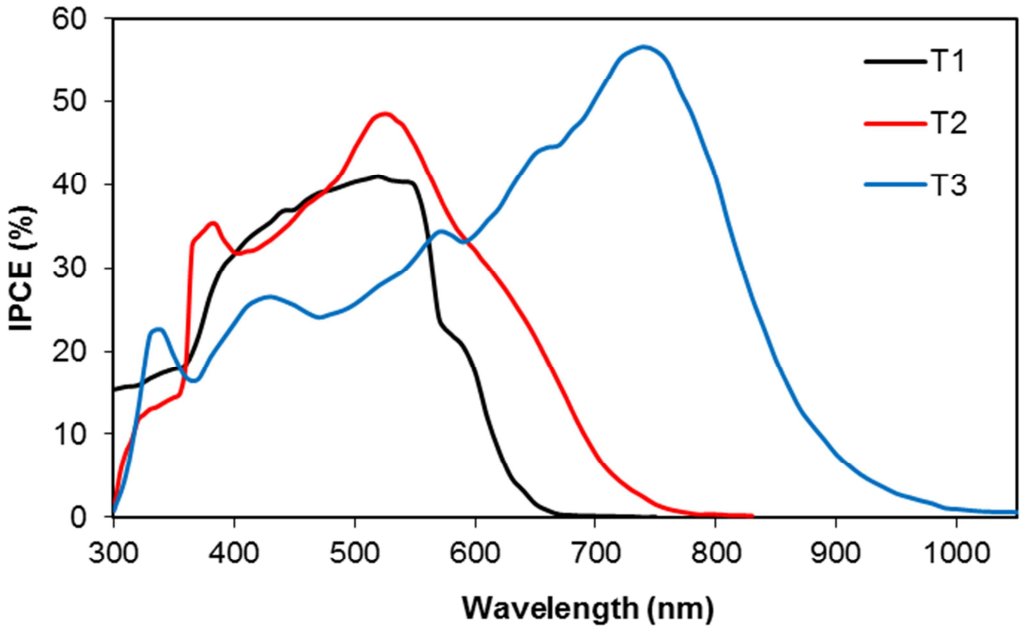

Fig. 7. The IPCE curves of the best performing devices described in Fig. 6.

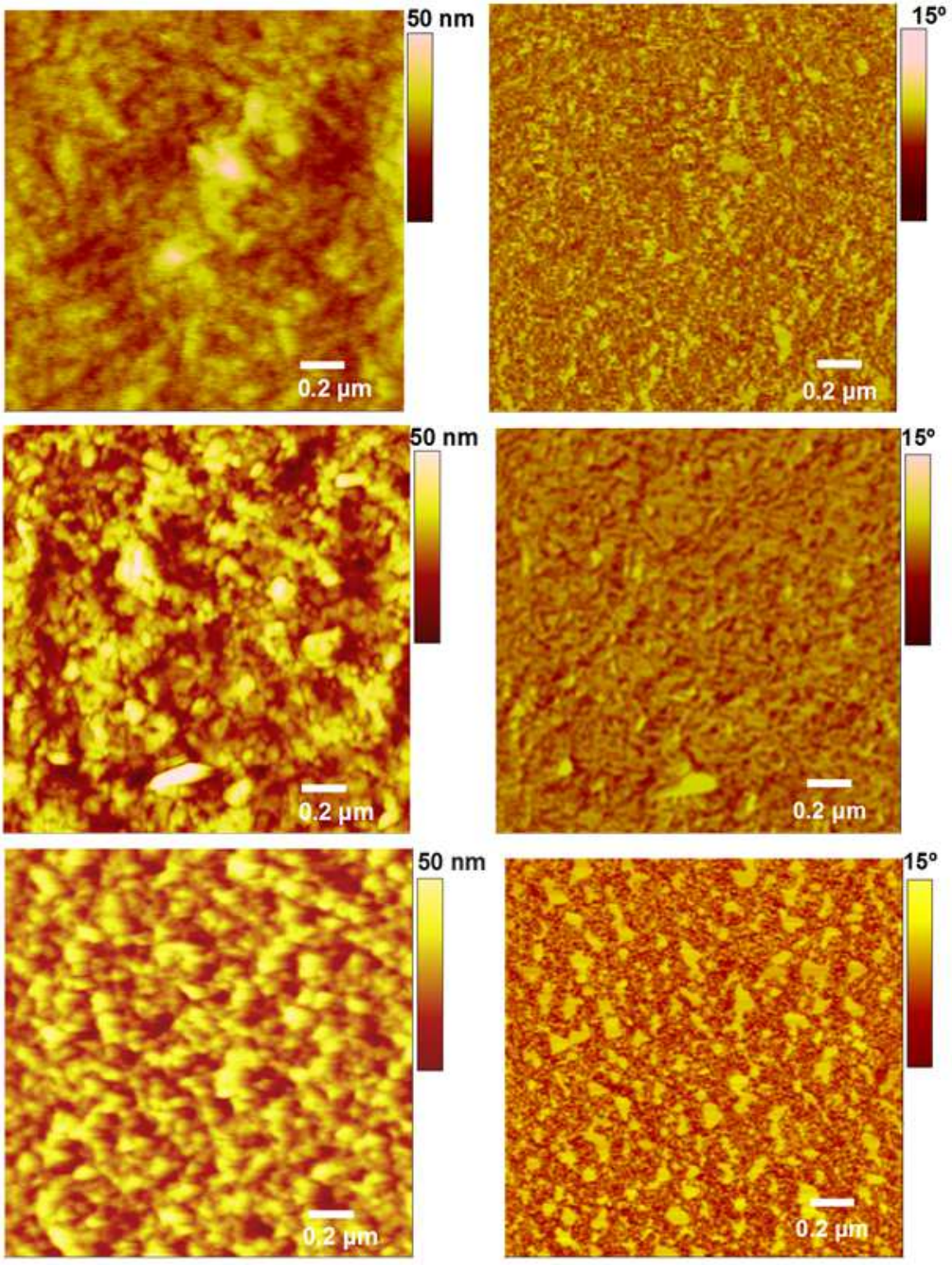

Fig. 8. AFM images of 1: 1 blend films with $PC_{61}BM$ spin-cast from chlorobenzene solutions on top of annealed ITO/PEDOT: PSS substrates. Topographic (left) and phase images (right) for **T1** (upper; roughness = 4.7 nm), **T2** (middle; roughness = 5.8 nm) and **T3** (lower; roughness = 3.9 nm) are depicted.

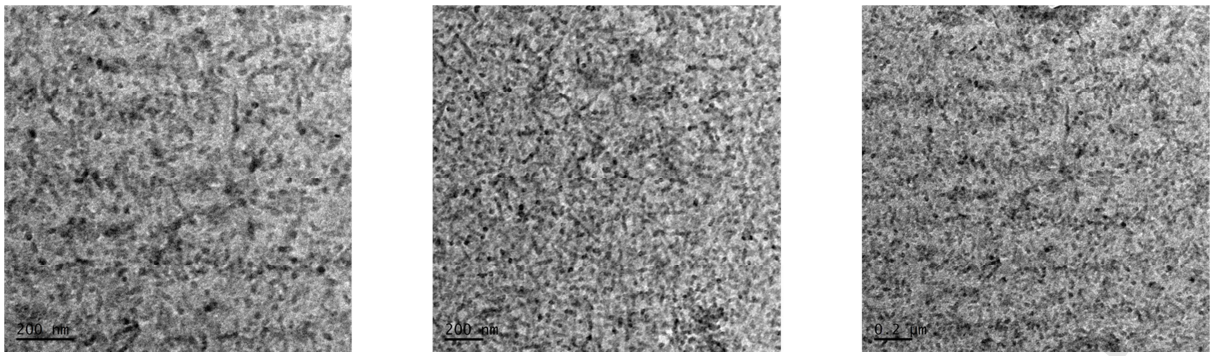

Fig. 9. TEM images for the blends of **T1**/**T2**/**T3**: $PC_{61}BM$ (1: 1; left to right, respectively) showing excellent mixing of donor and acceptor domains. For a better view, scale bar of 200 nm is represented.

Research Highlights

- First effort to expand the “push-pull” format based on direct connection of an amine to oligothiophene
- Combination of a ditolylamino donor unit with a variety of acceptors (cyanoacetate, cyanopyridone and dicyanoindenedione)
- The **T3**:$PC_{61}BM$-based device provided a PCE of 6.12%, the highest number for an unthrottled “push-pull” donor target
- Highly instructive work in the rational molecular design of small molecule donor chromophores